

Surface potential and magnetic properties of $\text{La}_{0.7}\text{Sr}_{0.3}\text{MnO}_3$ periodic arrays fabricated by direct electron beam writing

Ming-Chung Wu,^{1,a)} Yi-Jen Wu,¹ Yu-Ching Huang,¹ Chih-Min Chuang,¹
Kuo-Chung Cheng,² Ching-Fuh Lin,³ Yang-Fang Chen,^{4,5,a)} and Wei-Fang Su^{1,5,b)}

¹Department of Materials Science and Engineering, National Taiwan University, Taipei 106-17, Taiwan

²Department of Chemical Engineering and Biotechnology, National Taipei University of Technology, Taipei 106-08, Taiwan

³Graduate Institute of Electro-optical Engineering and Department of Electrical Engineering, National Taiwan University, Taipei 106-17, Taiwan

⁴Department of Physics, National Taiwan University, Taipei 106-17, Taiwan

⁵Center for Condensed Matter Sciences, National Taiwan University, Taipei 106-17, Taiwan

(Received 4 April 2008; accepted 18 May 2008; published online 29 July 2008)

It is demonstrated that magnetic periodic arrays can be easily fabricated from direct writing water developable $\text{La}_{0.7}\text{Sr}_{0.3}\text{MnO}_3$ electron beam resist. Two unique features of our approach are (1) the patterned $\text{La}_{0.7}\text{Sr}_{0.3}\text{MnO}_3$ resist film can be developed using nontoxic and environmentally friendly pure water and (2) either positive or negative patterns can be fabricated depending on the dosage of electron beam. The mechanism of the dual function characteristic of the resist was studied using Kelvin probe microscope. The surface potential of patterned $\text{La}_{0.7}\text{Sr}_{0.3}\text{MnO}_3$ resist increases with increasing electron beam dosage due to the changes of resist composition. The formations of periodic magnetic arrays were confirmed by the studies of scanning electron microscope and magnetic force microscope. The magnetization of $\text{La}_{0.7}\text{Sr}_{0.3}\text{MnO}_3$ can be enhanced by postsintering the sample at 900 °C after electron beam irradiation. We have therefore provided a one-step, simple, and convenient alternative technique for the fabrication of nanoscale magnetic patterns, which form the building blocks for the study of physical properties in periodic magnetic arrays. © 2008 American Institute of Physics. [DOI: 10.1063/1.2957489]

I. INTRODUCTION

Electron beam lithography is a technique to generate patterns on a surface using a beam of electrons. Although the pattern generating rate may appear not as fast as a parallel technique like photolithography, electron beam lithographic pattern can easily reach the nanoscale regime by controlling the electron beam width and can overcome the diffraction limit of light source.^{1,2} Resists are usually passive and have no specific function. If one can develop resists with active functions such as conductivity, luminescence, and magnetic properties, the fabrication process of specific devices can be simplified. However, relatively few active resists are reported. Clendennings *et al.*³ and Maclachlan *et al.*⁴ reported a direct writing of patterned ceramics using electron beam lithography and Co-PFS resist, and the resist could be used in spintronics as an isolating magnetic layer in a nanogranular in-gap structure. Pang *et al.*⁵ presented a method to produce a luminescent resist, polymethyl methacrylate (PMMA)-quantum-dot (QD) composite, by prepolymerized PMMA and colloidal semiconductor QDs. Song *et al.*⁶ reported in 2005 a nanoengineered fluorescent response from an active resist semiconductor core shell (CdSe/ZnS) QDs being close to the surface plasmon polariton field of the periodic Ag arrays. Saifullah *et al.*⁷ demonstrated a fabrication

of high aspect ratio ZnO structure by electron beam lithography, and the best photoluminescence characteristics of ZnO was exhibited after heat treated at 500 °C.

Recently, we have developed a water developable $\text{La}_{0.7}\text{Sr}_{0.3}\text{MnO}_3$ electron beam resist,⁸ which can be used to fabricate either positive or negative magnetic nanopatterns in one step. In this paper, we have further studied their surface potential behaviors using Kelvin probe force microscope (KFM) and magnetic properties of $\text{La}_{0.7}\text{Sr}_{0.3}\text{MnO}_3$ nanopatterns using magnetic force microscope (MFM). For MFM, nanoscale magnetic patterns^{9,10} or current flow distributions¹¹ can be profiled through the interaction between a magnetized tip and the sample surface. Moreover, for KFM, one can detect the surface potential from the work function difference between a noble metal-coated tip and the surface of materials and obtain the work function in an indirect way.^{12–15} The results of the surface potential of patterned $\text{La}_{0.7}\text{Sr}_{0.3}\text{MnO}_3$ by KFM confirm the mechanism of dual functional characteristics of the resist. The magnetic properties of the structure can be clearly detected by MFM. Our approach provides a simple and convenient alternative technique for the fabrication of nanoscale magnetic patterns, which form the building blocks for the study of physical properties in periodic magnetic array.

II. EXPERIMENTAL DETAILS

In this experiment, the electron beam resist was prepared by dissolving 4.50 wt % of lanthanum nitrate [$\text{La}(\text{NO}_3)_3 \cdot 6\text{H}_2\text{O}$, Acros, 98%], strontium hydroxide

^{a)}Electronic mail: yfchen@phys.ntu.edu.tw.

^{b)}Electronic mail: suwf@ntu.edu.tw.

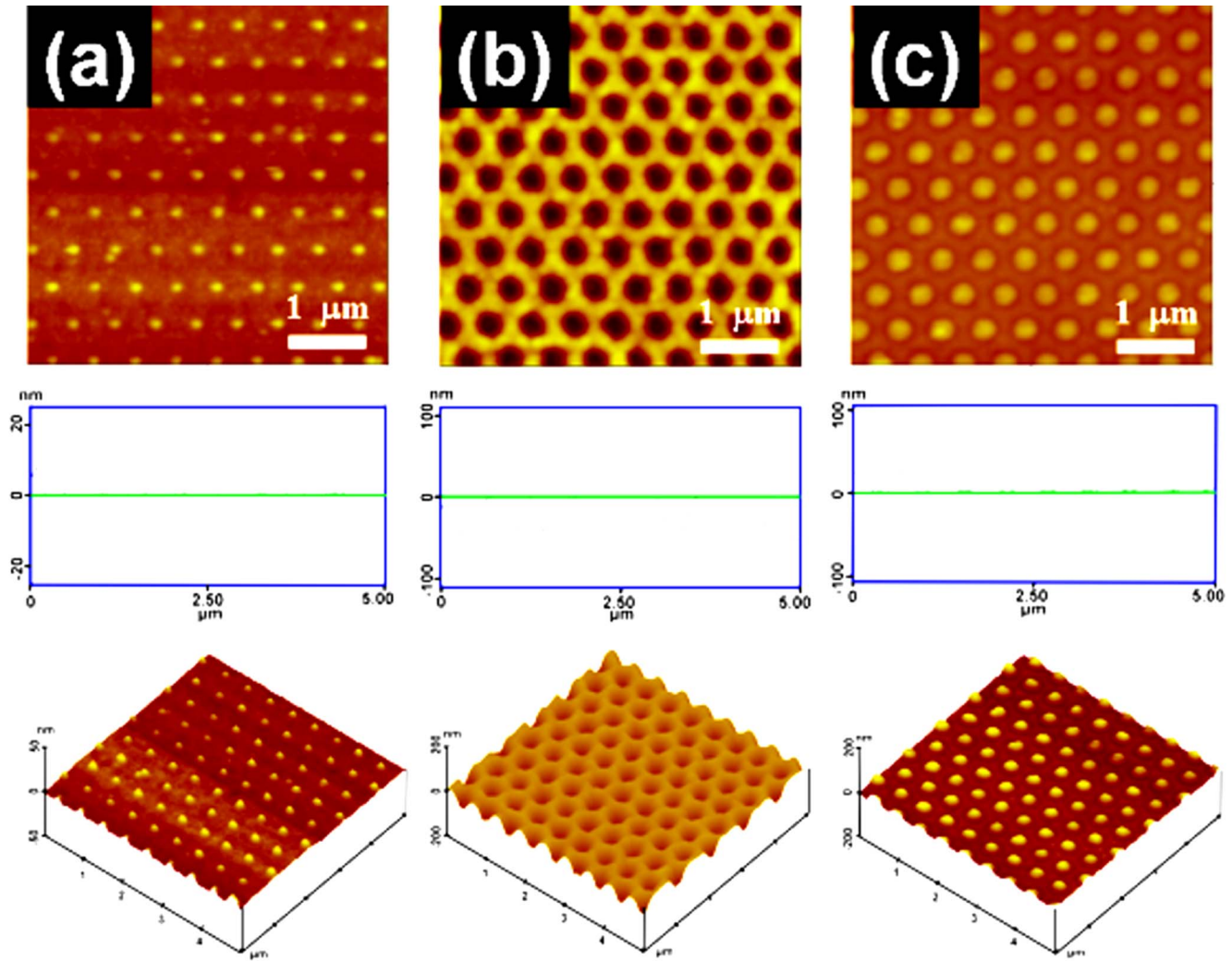


FIG. 1. (Color online) Two dimensional and three dimensional AFM topographic images and cross-section images of $\text{La}_{0.7}\text{Sr}_{0.3}\text{MnO}_3$ periodic arrays. (a) Negative $\text{La}_{0.7}\text{Sr}_{0.3}\text{MnO}_3$ periodical structure with low dosage (3.2 mC/cm^2) electron beam irradiation. (b) Positive $\text{La}_{0.7}\text{Sr}_{0.3}\text{MnO}_3$ periodical structure with medium dosage (32.0 mC/cm^2) electron beam irradiation. (c) Negative $\text{La}_{0.7}\text{Sr}_{0.3}\text{MnO}_3$ periodical structure with high dosage (233.6 mC/cm^2) electron beam irradiation. The scan size is $5 \times 5 \mu\text{m}^2$.

[$\text{Sr}(\text{NO}_3)_2$, Riedel-deHaen, p.a.], manganese nitrates [$\text{Mn}(\text{NO}_3)_2 \cdot 4\text{H}_2\text{O}$, Fluka, >97%], and 1.70 wt % polyvinyl alcohol (PVA) (Acros, 88%, 22 000 g/mol) in water with a molar ratio of La: Sr: Mn = 0.7:0.3:1. The solution was stirred for 48 h at 25°C . Then the $\text{La}_{0.7}\text{Sr}_{0.3}\text{MnO}_3$ material was spin coated at 3000 rpm for 90 s to give a nominal thickness of about 180 nm. High-resolution nanolithography was performed by writing specific patterns across the $150 \mu\text{m}$ field with a 2.5 nm beam step size using a Hitachi ELS-7500EX machine operating at 100 kV with a probe current of 1.0 nA. A sample containing a 3×3 array of field was exposed with a start dose of $1 \mu\text{s}$ then with an additional dose increments of 0.01, 0.1, and $1 \mu\text{s}$ per field, respectively. The exposed sample was then developed with pure water for 30 s. The patterned $\text{La}_{0.7}\text{Sr}_{0.3}\text{MnO}_3$ samples were measured by atomic force microscopy (AFM) (Digital Instruments, Dimension-3100 Multimode) for surface morphology and roughness, and the microstructures of the samples were observed by field emission scanning electron microscope (Elionix, ERA-8800FE, Japan). The magnetore-

sistance properties and magnetic properties were measured by physical property measurement system (Quantum Design, PPMS-9) and superconducting quantum interference devices (SQUID) (Quantum Design, MPMS-XL7), respectively. The surface potential and magnetic behavior distribution of the patterned $\text{La}_{0.7}\text{Sr}_{0.3}\text{MnO}_3$ were evaluated using KFM and MFM (Digital Instruments, Dimension-3100 Multimode).

III. RESULTS AND DISCUSSION

We have demonstrated that the water developable $\text{La}_{0.7}\text{Sr}_{0.3}\text{MnO}_3$ electron beam resist exhibits dual negative and positive patterning functions depending on the electron beam dosage. Figures 1(a)–1(c) are the two dimensional AFM images, cross-section images, and three dimensional AFM images of the $\text{La}_{0.7}\text{Sr}_{0.3}\text{MnO}_3$ periodic arrays on silicon wafer substrate fabricated using different electron beam dosages. Figure 1(a) is a negative pattern obtained at a low electron beam dose of 3.2 mC/cm^2 . Figure 1(b) is a positive pattern obtained at a medium electron beam dose of

32 mC/cm². At a high electron dose of 233.6 mC/cm², we obtained a negative pattern again. Although the dose of the exposure of this La_{0.7}Sr_{0.3}MnO₃ resist is relatively high in comparison to most organic resists, the La_{0.7}Sr_{0.3}MnO₃ resist generates active electromagnetic functional nanopatterns in one step, whereas the use of conventional organic resists to generate La_{0.7}Sr_{0.3}MnO₃ patterns involves three steps: (1) fabricate patterns from organic resist, (2) deposit La_{0.7}Sr_{0.3}MnO₃ on the patterns, and (3) remove organic resist. The use of La_{0.7}Sr_{0.3}MnO₃ electron beam resist will not only reduce process steps but also use no environmental harmful organic chemicals as compared to the organic resist. Our La_{0.7}Sr_{0.3}MnO₃ resist exhibits zwitterresist characteristics, so the height or depth in different patterns will vary with electron dose. The height of regular honeycomb array of La_{0.7}Sr_{0.3}MnO₃ pillars [Fig. 1(a)] is 10 nm, and the depth of positive pattern of regular honeycomb array is 50 nm [Fig. 1(b)]. Finally, the height of regular honeycomb array of La_{0.7}Sr_{0.3}MnO₃ pillars [Fig. 1(a)] is 40 nm.

We have previously illustrated that the formation of La_{0.7}Sr_{0.3}MnO₃ resist pattern is due to the heat from the electron beam exposure. Herein, we measure the surface potential of different La_{0.7}Sr_{0.3}MnO₃ patterns by KFM to confirm the formation of La_{0.7}Sr_{0.3}MnO₃ resist pattern. KFM has been widely used for the nanoscale mapping of surface potential differences and local dipoles that reveal important information on material properties. At the low electron dose (2.8 mC/cm²), only the exposed area is affected by the cross-linking of the PVA and results in a negative pattern of regular honeycomb array of La_{0.7}Sr_{0.3}MnO₃ pillars. At the low electron dose, the surface potential of the La_{0.7}Sr_{0.3}MnO₃ pillars consisting of nitrate salt and PVA is about 4.68 eV. At the medium dose (28.8 mC/cm²), the nitrate salt components of La_{0.7}Sr_{0.3}MnO₃ resist react with the PVA at the exposure area [Figs. 2(c) and 2(d)]. An explosive reaction occurs, the so-called autoignited combustion,¹⁶⁻¹⁸ and then the resist structure will change to form loose particles that can be easily removed by water to form positive pattern of regular triangular array [Figs. 2(c) and 2(d)]. The surface potential of the La_{0.7}Sr_{0.3}MnO₃ positive patterns consisting of nitrate salt and PVA at the medium dose is about 4.72 eV. The surface potential of the La_{0.7}Sr_{0.3}MnO₃ periodic array at medium dose (4.72 eV) is similar to the surface potential of periodic array at low dose (4.68 eV) because the chemical compositions of La_{0.7}Sr_{0.3}MnO₃ patterns at low or medium dose are similar. Finally, at the high dose (224 mC/cm²), the area exposed to the electron beam [Figs. 2(e) and 2(f)] shows a negative pattern with the formation of crystalline La_{0.7}Sr_{0.3}MnO₃. At or above this electron beam thermal energy threshold, the pure phase of La_{0.7}Sr_{0.3}MnO₃ formed as a solid pattern; the neighboring loose La_{0.7}Sr_{0.3}MnO₃ particle can be removed by water. The surface potential of the La_{0.7}Sr_{0.3}MnO₃ positive patterns at the high dose is about 4.80 eV, which is the same as the value reported in the literature.¹⁹⁻²³

Figure 3 reveals x-ray diffraction (XRD) patterns of the La_{0.7}Sr_{0.3}MnO₃ thin film sample sintered at different temperatures. All the peaks can be perfectly indexed as the pure rhombohedral phase [R $\bar{3}c(167)$] (Ref. 24) of La_{0.7}Sr_{0.3}MnO₃

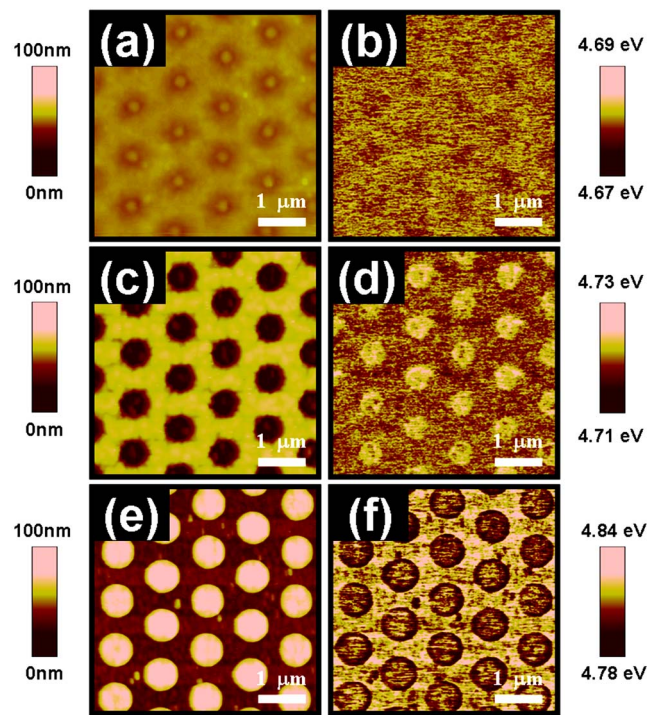


FIG. 2. (Color online) Topographic images (a, c, e) and KFM images (b, d, f) of La_{0.7}Sr_{0.3}MnO₃ periodic arrays. (a,b) Negative La_{0.7}Sr_{0.3}MnO₃ periodical structure with low dosage (2.8 mC/cm²) electron beam irradiation. (c,d) Positive La_{0.7}Sr_{0.3}MnO₃ periodical structure with medium dosage (28.8 mC/cm²) electron beam irradiation. (e,f) Negative La_{0.7}Sr_{0.3}MnO₃ periodical structure with high dosage (224.0 mC/cm²) electron beam irradiation. The scan size is 5 × 5 μm².

with lattice constants $a=5.09$ Å and $c=13.37$ Å. The sample sintered at 300 °C clearly indicates the formation of high symmetry pseudocubic phase of La(Sr)MnO₃ containing trace amounts of MnO₂ and La₂O₃ impurity phases. The sample sintered at 900 °C indicates the change from impurity phase to a rhombohedral form of the perovskitelike structure. Therefore, the patterned La_{0.7}Sr_{0.3}MnO₃ was postsintered at 900 °C to obtain the pure rhombohedral phase for high magnetic susceptibility.

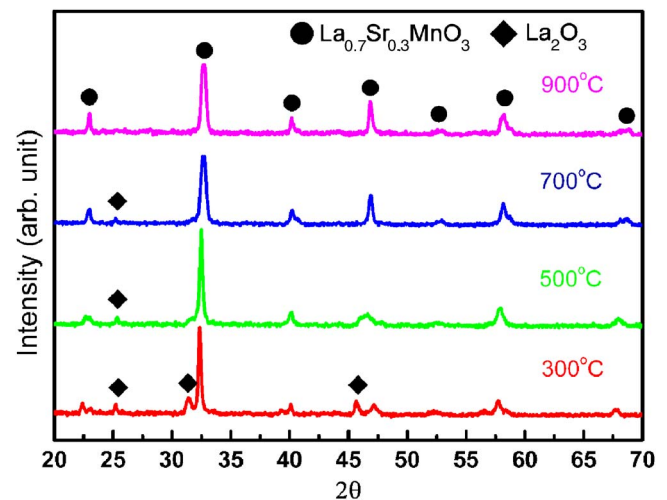


FIG. 3. (Color online) XRD patterns of water developable La_{0.7}Sr_{0.3}MnO₃ electron beam resist material sintered at different temperatures for 4 h.

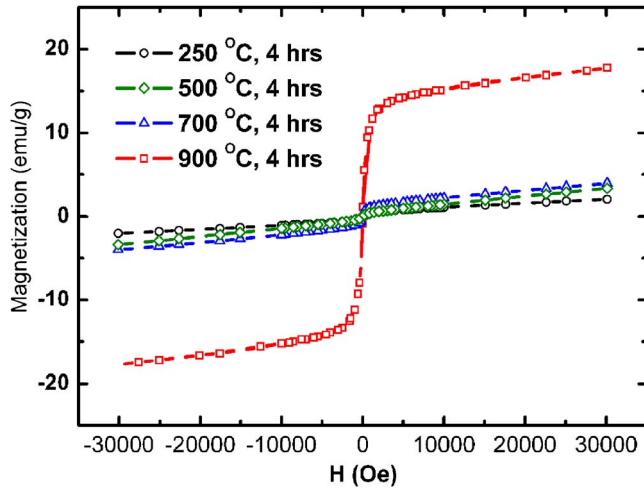
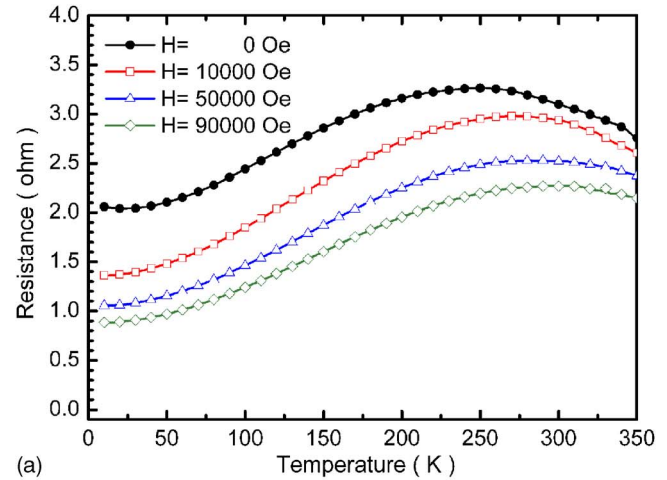


FIG. 4. (Color online) The hysteresis curves of water developable $\text{La}_{0.7}\text{Sr}_{0.3}\text{MnO}_3$ electron beam resist material sintered at different temperatures for 4 h are measured under 30 000 Oe at 300 K.

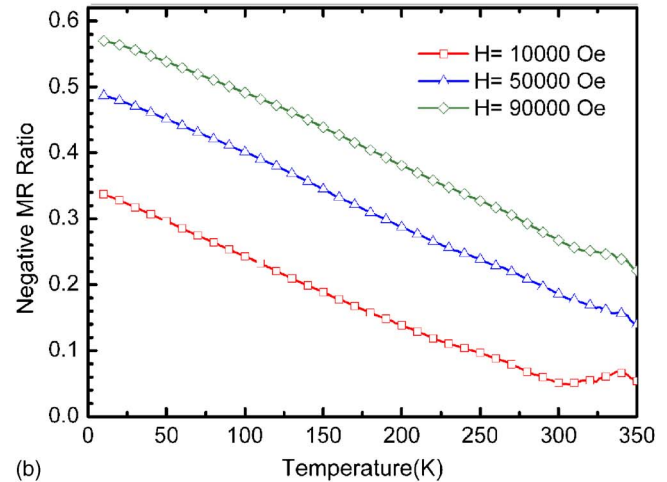
The $\text{La}_{0.7}\text{Sr}_{0.3}\text{MnO}_3$ powders sintered at different temperatures were measured by SQUID at 300 K, as shown in Fig. 4. The magnetization of $\text{La}_{0.7}\text{Sr}_{0.3}\text{MnO}_3$ powders sintered at 250, 500, and 700 °C almost have the similar saturation magnetization value of ± 3 emu/g at saturated magnetic susceptibility under 30 000 Oe at 300 K. However, the $\text{La}_{0.7}\text{Sr}_{0.3}\text{MnO}_3$ powder sample sintered at 900 °C exhibits saturation magnetization of ± 18 emu/g at saturated magnetic susceptibility under 30 000 Oe at 300 K. This shows that the magnetization of $\text{La}_{0.7}\text{Sr}_{0.3}\text{MnO}_3$ at saturated magnetic susceptibility changes with different sintering temperatures. Moreover, the differences of saturation magnetization of $\text{La}_{0.7}\text{Sr}_{0.3}\text{MnO}_3$ at saturated magnetic susceptibility are because of the formation of pure $\text{La}_{0.7}\text{Sr}_{0.3}\text{MnO}_3$ crystalline phase. The $\text{La}_{0.7}\text{Sr}_{0.3}\text{MnO}_3$ powder sample sintered at 900 °C for 4 h exhibits the highest magnetization among all the powder samples at saturated magnetic susceptibility because the sample forms a pure $\text{La}_{0.7}\text{Sr}_{0.3}\text{MnO}_3$ crystalline phase.

The magnetoresistance properties of the water developable $\text{La}_{0.7}\text{Sr}_{0.3}\text{MnO}_3$ resist were studied for powdered samples because the electron beam samples were too small to be studied by SQUID. The powder was prepared by drying the resist material at 120 °C for 12 h and sintered at 900 °C for 4 h. The magnetoresistance properties of the resist material were studied at different temperatures and different magnetic fields as shown in Figs. 5(a) and 5(b). The water developable $\text{La}_{0.7}\text{Sr}_{0.3}\text{MnO}_3$ material exhibits negative magnetoresistance effects. The resistance of the material decreases inversely with the external magnetic field and increases as the temperature increases up to 250 K. However, the resistance (Ω) at low temperature (~ 25 K) increases slightly due to the Coulomb barriers that exist on the grain boundary, hindering electron transport.

Figures 6(a) and 6(b) show scanning electron microscopy (SEM) images of $\text{La}_{0.7}\text{Sr}_{0.3}\text{MnO}_3$ material exposed to an electron beam followed by 4 h of sintering at 900 °C, which produces a honeycomb style periodic pattern, with their lattice constants of 600 nm. The $\text{La}_{0.7}\text{Sr}_{0.3}\text{MnO}_3$ mate-



(a)



(b)

FIG. 5. (Color online) The magnetoresistance properties of water developable $\text{La}_{0.7}\text{Sr}_{0.3}\text{MnO}_3$ electron beam resist material sintered at 900 °C for 4 h are measured under 30 000 Oe at 300 K. (a) The relationship between resistance and temperature at various magnetic fields and (b) the relationship between the magnetoresistance ratio and temperature at various magnetic fields.

rial exhibits positive resist characteristic [Fig. 6(a)] and negative resist characteristic [Fig. 6(b)]. Figure 6(c) shows a SEM image of $\text{La}_{0.7}\text{Sr}_{0.3}\text{MnO}_3$ material sintered at 900 °C for 4 h with a square periodic pattern and positive resist characteristic, and its lattice constant is 400 nm. The sample patterns remain despite being post-treated at high temperature. These results illustrate the dual functional characteristic of water developable $\text{La}_{0.7}\text{Sr}_{0.3}\text{MnO}_3$ materials and its capability to be either positive or negative by varying the electron doses. Figure 6(d) shows the energy dispersive x-ray spectroscopy (EDS) analysis of the patterned $\text{La}_{0.7}\text{Sr}_{0.3}\text{MnO}_3$ material sintered at 900 °C for 4 h. The atomic ratio of La, Sr, and Mn is approximately 0.7:0.3:1.0. This result indicates that the fabrication process does not alter the initial reactants' mixing ratio.

The nanoscale magnetic properties of water developable $\text{La}_{0.7}\text{Sr}_{0.3}\text{MnO}_3$ electron beam resist material were studied by MFM. MFM equips a scanning probe microscope that can map the spatial distribution of magnetism by measuring the magnetic interaction between a sample and a tip. Figure 7 (a~j) shows AFM topographic images and magnetic force

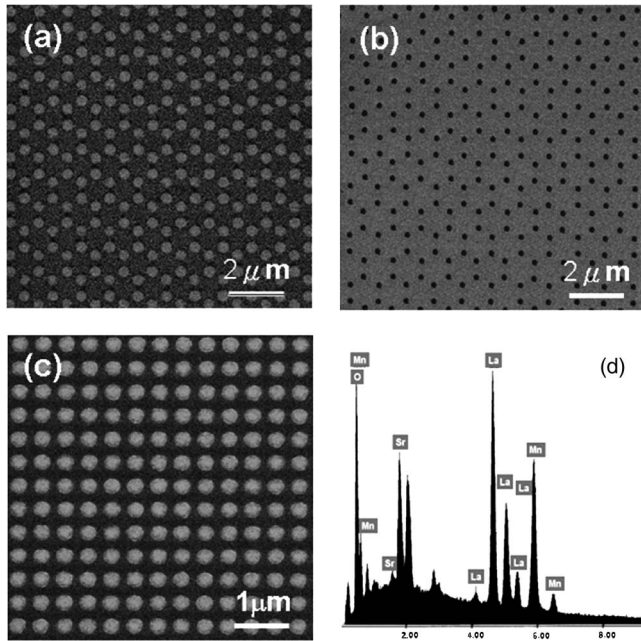


FIG. 6. SEM images of $\text{La}_{0.7}\text{Sr}_{0.3}\text{MnO}_3$ periodic arrays exposed to the electron beam plus 4 h sintering at 900°C . (a) Honeycomb periodic pattern with positive resist characteristic, (b) honeycomb periodic pattern with negative resist characteristic, (c) square periodic pattern with positive resist characteristic, and (d) EDS analysis of the patterned $\text{La}_{0.7}\text{Sr}_{0.3}\text{MnO}_3$ material sintered at 900°C for 4 h, showing the presence of La, Sr, Mn, and O.

gradient images (phase signal) of the samples. These images are $2 \times 5 \mu\text{m}^2$, and their data scales are 100 nm and 20° , respectively. In MFM mode, the cantilever is lifted up 25 nm higher than in the topography mode. Figures 7(a) and 7(b) illustrate the topographic image and magnetic force gradient image of a sample with regular triangular pillar array (600 nm in diameter, $1.0 \mu\text{m}$ lattice constant, and 50 nm thick). The sample was produced by exposing the resist to an electron dose of $224.0 \text{ mC}/\text{cm}^2$ without postsintering treatment. Figures 7(c) and 7(d), 7(e) and 7(f), and 7(g) and 7(h) show the regular triangular $\text{La}_{0.7}\text{Sr}_{0.3}\text{MnO}_3$ pillar array sintered at 300, 500, and 700°C for 4 h, respectively. For the samples postsintered at 300, 500, 700°C , the sizes of $\text{La}_{0.7}\text{Sr}_{0.3}\text{MnO}_3$ pillar array decrease slightly with the increasing postsintering temperature, and the MFM phase shift signals are becoming obscure. The result indicates that MFM contrasts come from the atomic force distribution in the samples rather than the magnetic force distribution for these samples sintered below 700°C . However, the $\text{La}_{0.7}\text{Sr}_{0.3}\text{MnO}_3$ pillar array with postsintering at 900°C for 4 h shows clear MFM signals; it indicates that MFM images are due to the magnetic force distribution in the sample rather than the atomic force. From the data presented, it can be derived that the MFM behavior of $\text{La}_{0.7}\text{Sr}_{0.3}\text{MnO}_3$ array occurred due to the formation of pure $\text{La}_{0.7}\text{Sr}_{0.3}\text{MnO}_3$ crystalline phase. The finding also corresponds to the previous XRD and SQUID study.

To further confirm that the MFM images are indeed owing to the magnetic force distribution instead of van der Waals forces, we performed various MFM measurements by changing the tip-sample separation distance (lift scan height). The principle of MFM measurement is based on

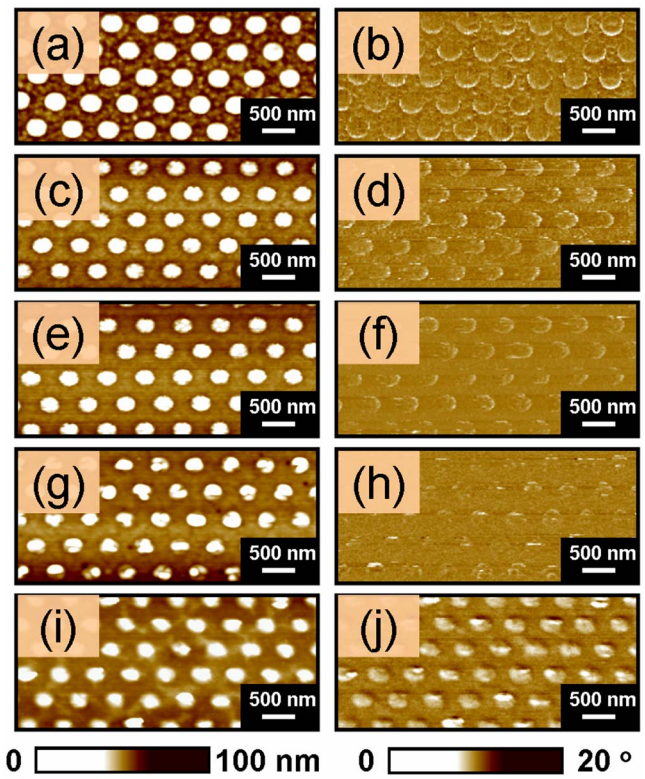


FIG. 7. (Color online) MFM images of $\text{La}_{0.7}\text{Sr}_{0.3}\text{MnO}_3$ periodic arrays. [(a) and (b)] Topographic image and phase shift image, respectively, of sample prepared at $233.6 \text{ mC}/\text{cm}^2$ electron exposure plus postsintering with a triangular holes array with a 600 nm diameter, 1000 nm lattice constant, and 40 nm thickness, [(c) and (d)] after electron beam irradiation plus 300°C postsintering, [(e) and (f)] after electron beam irradiation plus 500°C postsintering, [(g) and (h)] after electron beam irradiation plus 700°C postsintering, and [(i) and (j)] after electron beam irradiation plus 900°C postsintering. The data scales of these images are 100 nm and 20° , respectively.

noncontact AFM. Therefore, both the atomic force and the magnetic interactions are detected. From the aspect of atomic force, neutral atoms and molecules are subject to two distinct forces correlating to large and short distances. The attractive force is at long ranges and a repulsive force is at short ranges. The Lennard-Jones²⁵ potential is a simple mathematical model that represents this behavior as [Eq. (1)]

$$V(r) = 4\epsilon \left[\left(\frac{\sigma}{r} \right)^{12} - \left(\frac{\sigma}{r} \right)^6 \right], \quad (1)$$

where ϵ is the depth of the potential well, r is the distance between two neutral atoms or two molecules, and σ is the finite distance at which the potential is zero. These parameters can be fitted to reproduce experimental data or deduced from the results of accurate quantum chemistry calculations. The term $(1/r)^{12}$ describes repulsion and the term $(1/r)^6$ describes attraction. The force function is the negative of the gradient of the above potential, which is given by

$$F(r) = -\frac{d}{dr}V(r)\hat{r} = 4\epsilon \left[12\frac{\sigma^{12}}{r^{13}} - 6\frac{\sigma^6}{r^7} \right] \hat{r}. \quad (2)$$

The magnetic force equation between two poles abides by Coulomb's law and follows

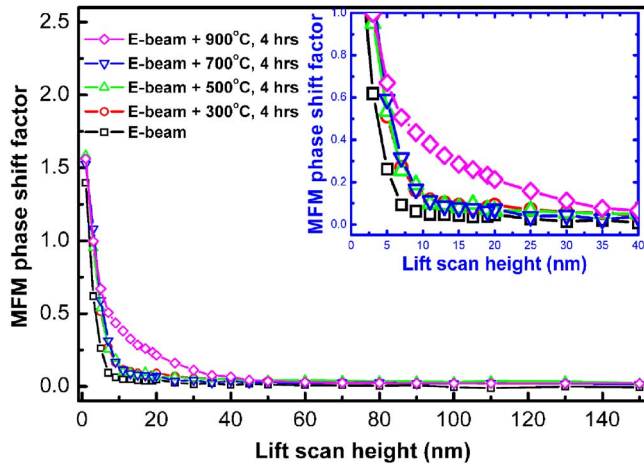


FIG. 8. (Color online) The phase shift factors of $\text{La}_{0.7}\text{Sr}_{0.3}\text{MnO}_3$ periodic arrays at different scanning heights in MFM measurement.

$$F = \frac{p_1 p_2}{4\pi\mu_0 r^2}, \quad (3)$$

where r is the distance between two poles, p_1 and p_2 are poles, and μ_0 is the permeability of empty space that is equal to $4\pi \times 10^{-7}$ Wb/A m. Thus, we can see that the van der Waals force decreases with increasing distance more rapidly than the magnetic force. Figure 8 shows the phase shift factor, which is proportional to the force acting on the tip, at different tip-sample distances in the MFM and AFM measurements for the samples with different postsintering. The sample with post-900 °C-sintering treatment exhibits a slow force that decreases with increasing tip-sample distance, indicating that the sample has a large magnetic moment. Whereas, the samples with post-low-sintering treatment (<700 °C) or without postsintering treatment have negligible magnetic moment and exhibit a force that decreases drastically with increasing the tip-sample distance. At small tip-sample distances ($\ll 10$ nm), the total force is dominated by the atomic force, and the difference between the MFM and AFM phase images is indistinguishable. When the distance is greater than 10 nm, the magnetic force becomes dominant. Both forces diminish after the distance exceeds 30 nm. The overall trend of two experimental curves is seen to be described quite well by Eqs. (2) and (3). We therefore conclude that a well-defined magnetic pattern has been fabricated using water developable $\text{La}_{0.7}\text{Sr}_{0.3}\text{MnO}_3$ electron beam resist.

IV. CONCLUSIONS

In summary, we have created magnetic patterns using water developable $\text{La}_{0.7}\text{Sr}_{0.3}\text{MnO}_3$ electron beam resist in an environmentally friendly one-step method, and both positive and negative patterns are ready to be fabricated by only varying electron dose. The surface potential of patterned $\text{La}_{0.7}\text{Sr}_{0.3}\text{MnO}_3$ measured by KFM is very useful to identify the chemical compositions and mechanism of the dual function of $\text{La}_{0.7}\text{Sr}_{0.3}\text{MnO}_3$ resist. The magnetic properties of the

patterned $\text{La}_{0.7}\text{Sr}_{0.3}\text{MnO}_3$ can be clearly observed by postsintering the sample at 900 °C for 4 h after electron beam writing. We would like to stress that our study provides a simple and convenient approach for the fabrication of magnetic patterns, which underpin many interesting physical properties awaiting future explorations.

ACKNOWLEDGMENTS

Financial support obtained from the National Science Council of Taiwan (Project Nos. NSC95-3114-P-002-003-MY3 and NSC96-2628-E-002-017-MY3) is highly appreciated. The authors also thank Professor C. H. Kuan, Professor C. W. Chen, Mr. Y. Y. Lin, Ms. S. Chen, and Mr. J. F. Lin of National Taiwan University for helpful discussions and Mr. A. J. Su of University of Pittsburgh for editing the manuscript. The electron beam lithography was carried out using the Elinox's facility located in the National Taiwan University Center for Information and Electronics Technologies.

- ¹C. S. Wu, C. F. Lin, H. Y. Lin, C. L. Lee, and C. D. Chen, *Adv. Mater. (Weinheim, Ger.)* **19**, 3052 (2007).
- ²H. Y. Lin, L. C. Tsai, P. Y. Chi, and C. D. Chen, *Adv. Mater. (Weinheim, Ger.)* **18**, 1517 (2006).
- ³S. B. Clendenning, S. Aouba, M. S. Rayat, D. Grozen, J. B. Sorge, P. M. Broderson, R. N. S. Sodhi, Z.-H. Lu, C. M. Yip, M. R. Freeman, H. E. Ruda, and I. Manners, *Adv. Mater. (Weinheim, Ger.)* **16**, 215 (2004).
- ⁴M. J. MacLachlan, M. Ginzburg, N. Coombs, T. W. Coyle, N. P. Raju, J. E. Greedan, G. A. Ozin, and I. Manners, *Science* **287**, 1460 (2000).
- ⁵L. Pang, Y. Shen, K. Tetz, and Y. Fainman, *Opt. Express* **13**, 44 (2005).
- ⁶J. Song, T. Atay, S. Shi, H. Urabe, and A. V. Nurmikko, *Nano Lett.* **5**, 1557 (2005).
- ⁷M. S. M. Saifullah, K. R. V. Subramanian, D.-J. Kang, D. Anderson, W. T. S. Huck, G. A. C. Jones, and M. E. Welland, *Adv. Mater. (Weinheim, Ger.)* **17**, 1757 (2005).
- ⁸M. C. Wu, C. M. Chuang, Y. F. Chen, and W. F. Su, *J. Mater. Chem.* **18**, 780 (2008).
- ⁹I. C. Chen, L. H. Chen, A. Gapin, S. Jin, L. Yuan, and S. H. Liou, *Nanotechnology* **19**, 075501 (2008).
- ¹⁰H. Kuramochi, T. Uzumaki, M. Yasutake, A. Tanaka, H. Akinaga, and H. Yokoyama, *Nanotechnology* **16**, 24 (2005).
- ¹¹F. Král, D. Perednis, B. Huey, D. A. Bonnell, G. Kostorz, and L. J. Gauckler, *Adv. Mater. (Weinheim, Ger.)* **10**, 1442 (1998).
- ¹²H. Hoppe, T. Glatzel, M. Niggemann, A. Hinsch, M. C. Lux-Steiner, and N. S. Sariciftci, *Nano Lett.* **5**, 269 (2005).
- ¹³H. O. Jacobs, P. Leuchtman, O. J. Homan, and A. Stemmer, *J. Appl. Phys.* **84**, 1168 (1998).
- ¹⁴Z. Yang and M. G. Spencer, *Appl. Phys. Lett.* **89**, 263504 (2006).
- ¹⁵B. Pérez-García, J. Abad, A. Urbina, J. Colchero, and E. Palacios-Lidón, *Nanotechnology* **19**, 065709 (2008).
- ¹⁶H. B. Park, H. J. Kweon, Y. S. Hong, S. J. Kim, and K. Kim, *J. Mater. Sci.* **32**, 57 (1997).
- ¹⁷S. K. Behera, P. Barpanda, S. K. Pratihari, and S. Bhattacharyya, *Mater. Lett.* **58**, 1451 (2004).
- ¹⁸C. M. Chuang, M. C. Wu, Y. C. Huang, Y. F. Chen, C. F. Lin, and W. F. Su, *Nanotechnology* **17**, 4399 (2006).
- ¹⁹T. Kudo, M. Tachiki, T. Kashiwai, and T. Kobayashi, *Jpn. J. Appl. Phys., Part 2* **37**, L999 (1998).
- ²⁰S. Yunoki, A. Moreo, E. Dagotto, S. Okamoto, S. S. Kancharla, and A. Fujimori, *Phys. Rev. B* **76**, 064532 (2007).
- ²¹I. Bergenti, V. Dediu, M. Murgia, A. Riminucci, G. Ruani, and C. Taliani, *J. Lumin.* **110**, 384 (2004).
- ²²E. Arisi, I. Bergenti, V. Dediu, M. A. Loi, M. Muccini, M. Murgia, G. Ruani, C. Taliani, and R. Zamboni, *J. Appl. Phys.* **93**, 7682 (2003).
- ²³D. W. Reagor, S. Y. Lee, Y. Li, and Q. X. Jia, *J. Appl. Phys.* **95**, 7971 (2004).
- ²⁴JCPDS Card No. 89-8098 (2003)
- ²⁵J. E. Lennard-Jones, *Proc. Phys. Soc. London* **43**, 461 (1931).